Resonant inter-valence-band Raman scattering of photoexcited holes in germanium

Koichiro Tanaka, Hideyuki Ohtake,* and Tohru Suemoto
Institute for Solid State Physics, University of Tokyo, Tokyo 106, Japan
(Received 28 March 1994)

We have observed broad Raman scattering around 1500 cm^{-1} in undoped, n-type ($N_e = 10^{17}$ cm^{-3}) and p-type ($N_h = 10^{17}$ cm^{-3}) germanium crystals at room temperature when stimulated by the ~1.5-eV laser light. The integrated intensity of the Raman scattering has a square-law power dependence at high excitation densities above 0.5 kW/cm^2. This power dependence suggests that the origin of the scattering should be related to some photoexcited product. Since the power dependence becomes linear below 0.5 kW/cm^2 only in the p-type sample, the origin of the Raman scattering is attributed to holes in the valence band. The intensity of the Raman scattering is found to decrease rapidly at low temperatures. The peak position and the temperature dependence of the 1500 cm^{-1} component are successfully explained by a model based on k conserving resonant inter-valence-band Raman scattering of photoexcited holes.

I. INTRODUCTION

The inelastic scattering of light (Raman scattering) in solids originates from a number of processes including scattering by elementary excitations such as phonons, magnons, and plasmons. In heavily doped semiconductors, Raman scattering by single particle excitations has been observed in several solids.[1–10] The origins of this scattering fall into two broad categories: intraband nature and interband nature. In the former category, it is well known that several mechanisms–such as charge-density fluctuation (CDF), spin-density fluctuation (SDF), and intervalley-density fluctuation (IVF)–play an important role in the light-scattering processes.[11] In typical group-IV materials, such as Ge and Si, the bottom of the conduction band exists in a valley away from the zone center, and therefore IVF gives rise to the scattering in n-type samples.[1–7] On the other hand, their valence band typically consists of three components near the band edge with the heavy-hole (HH) and the light-hole (LH) bands degenerating at the Γ point, and another band (SO) splits off by spin-orbit splitting Δ. Reflecting the valence band structure, inter-valence-band Raman scattering (IVRS) has been observed in p-type semiconductors.[8–10] This interband scattering process reflects hole density fluctuation among valence bands.

In p-type Si[8] and p-type Ge,[9] nonresonant IVRS was observed as a broad spectrum which reflects the density of states and the Fermi level of holes. In p-type GaAs, Olego *et al.* measured resonant IVRS under the excitation of several Ar^+ laser lines.[10] They found that Raman scattering appears in the Stokes region from 2000 to 3600 cm^{-1} and that the shift depends on the laser frequency. To account for the scattering mechanism, they assumed that the electrons are photoexcited from the LH band to the intermediate states in the conduction band and make non-k-conserving (indirect) transition to the empty valence states in the HH band near the Fermi level. They assumed that the non-k-conserving process came from the high impurity density of their sample (N_h=9×10^{19} cm^{-3}).

In this study, we measured Raman scattering in Ge crystals. We generated electrons and holes by photoexcitation with the same laser to observe the Raman scattering. Reflecting the long carrier lifetime of Ge (longer than 1 μs at 300 K), the photoexcited carrier density was estimated to be ~10^{18} cm^{-3} at maximum. Along with the scattering from electrons in L valleys reported earlier,[5–7] we observed a broad band around 1500 cm^{-1} under excitation of ~1.5-eV laser light. In order to confirm the origin of the scattering, we measured the laser power dependence of the scattering intensity in several samples with different doping conditions. We also measured the peak shift of the 1500-cm^{-1} component while varying the laser frequency and the temperature dependence of the Raman scattering intensity while reducing the sample temperature from room temperature (RT) to liquid-nitrogen temperature (LNT). From the results of these experiments and their correspondence to band calculation results based on the $\vec{k}\cdot\vec{p}$ method, we conclude that the scattering around 1500 cm^{-1} originates from the k conserving resonant IVRS of photoexcited holes.

II. EXPERIMENT

We investigated the behavior of an undoped Ge sample with a (100) face at temperatures ranging from RT to LNT. We also evaluated a p-type Ge:In crystal (N_h=$10^{17}cm^{-3}$) and a n-type Ge:Sb crystal (N_e=$10^{17}cm^{-3}$) with a (100) face. The surfaces of the samples were polished by alumina polishing suspensions and etched in a dilute hydrofluoric acid. To measure the temperature dependence, we mounted the samples in a flow-type He cryostat. We used a cw Ti:sapphire laser (SP3900S) as a tunable excitation light source. The av-

erage power of this laser could be continuously varied by the combination of a polarization rotator (Fresnel rhomb retarder) and a linear polarizer. The background fluorescence of the laser was eliminated by a prism monochromator. The laser beam was focused onto the sample by a spherical achromatic lens ($f = 30$ or 60 mm) with a spot diameter of 40~50 μm. The scattered light was collected in a back scattering geometry by a camera lens (Nikon 50 mm, F1.2) and dispersed by a single monochromator (SPEX, 270M, $f = 27$ cm) with a Raman notch filter (Super notch filter, Kaiser Op. Systems, Inc.). Raman signals were detected by a liquid-nitrogen-cooled charge-coupled-device detector (SPEX, Spectrum One). Considering the large spectral width of the IVRS (~500 cm^{-1}) and the efficiency of the measurement, we used a 300-grooves/mm grating which reduces the spectral resolution but allows us to cover a wide range in a single measurement. In this study, the resolution of the monochromator was 1.6 nm which corresponds to 24 cm^{-1} at 800 nm. The obtained spectra were corrected for the instrumental response and the ordinate scale in the figures is proportional to the photon number per unit energy interval.

III. RESULTS

Figure 1 shows the typical polarized Raman spectrum of an undoped Ge sample under continuous wave (cw) excitation of 1.58-eV laser light with a power density of 4 kW/cm^2. The incident laser light was polarized parallel to the ⟨110⟩ axis of the crystal, and the polarization of the scattered light was set to be parallel to that of the incident laser light. Three scattering components can be seen: One due to LO phonons, which produce sharp lines at ±300 cm^{-1} and the two-LO-phonon scattering lines around ±600 cm^{-1}; another centered at 0 cm^{-1} which mainly originates from the intervalley density fluctuation (IVF) of photoexcited electrons in L valleys;[5–7] and a third component which has a peak around 1500 cm^{-1} with a broad bandwidth (~500 cm^{-1}). We can determine the true sample temperature by measuring the ratio of the intensities of the anti-Stokes- and Stokes-LO-phonon scattering by using

$$\frac{I_{\text{anti-Stokes}}}{I_{\text{Stokes}}} = \exp\left(-\frac{\varepsilon_{\text{LO}}}{k_B T}\right). \quad (1)$$

Under 4 kW/cm^2 excitation, the temperature of the sample was found to increase from 300 K to 311 K. We confirmed that the increase of temperature has little effect on the intensity of the 1500-cm^{-1} scattering. We also measured depolarized Raman spectra by rotating the polarization analyzer until it was perpendicular to the polarization of the incident laser. The Raman intensity of the 1500-cm^{-1} component in the depolarized polarization configuration is found to be half of that in the polarized configuration, indicating that the scattered light is slightly polarized as is usually expected for electronic Raman scattering due to CDF.[11]

Figure 2 shows Raman spectra obtained under excitation at different energies. The laser photon energy differs by 100 meV (807 cm^{-1}) between 1.483 eV (a) and 1.583 eV (d). The positions of the 1500-cm^{-1} peaks are summarized in Table I, and are almost constant with respect to the photon energy of the exciting laser. This result confirms that the observed 1500-cm^{-1} component is not luminescence but Raman scattering. However, it has a weak dependence on the excitation laser photon energy: the peak position of the 1500-cm^{-1} component increases by about 135 cm^{-1} as the laser photon energy increases

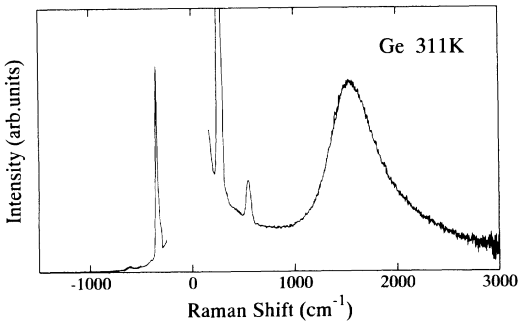

FIG. 1. Typical Raman spectrum of an undoped Ge sample at 311 K under cw excitation of 1.58-eV light with a density of 4 kW/cm^2. Polarization of the scattered light was taken to be parallel to that of the incident laser (parallel to the ⟨110⟩ crystal axis). The lack of data around 0 cm^{-1} is due to the Raman notch filter. The spectral resolution is about 24 cm^{-1}. The sample temperature was determined by using the anti-Stokes vs Stokes ratio of the LO-phonon scattering intensities (±300 cm^{-1}).

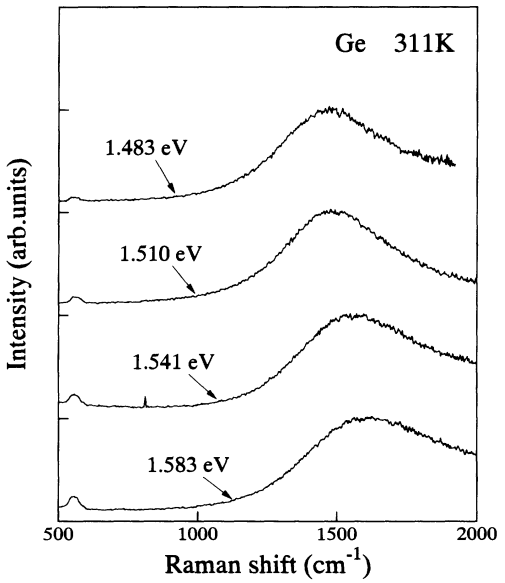

FIG. 2. Excitation photon energy dependence of the 1500-cm^{-1} Raman component. As the excitation photon energy is increased, the 1500-cm^{-1} component slightly shifts to the high energy side, whereas the two-LO-phonon scattering (~600 cm^{-1}) is the same in all spectra.

TABLE I. Peak positions of the IVRS vs excitation positions.

	Experiment (cm^{-1})	Calculation (cm^{-1})			
		k conserving		non-k-conserving	
Excitation energy (eV)		⟨100⟩	⟨111⟩	⟨100⟩	⟨111⟩
1.483	1410±10	1221	1328	1905	1594
1.510	1445	1237	1340	1954	1622
1.541	1500	1254	1359	2008	1655
1.583	1545	1276	1369	2084	1697

by ~800 cm^{-1}. This result is quite similar to the results of intervalence band Raman scattering measurements in p-type GaAs.[10]

We measured the spectra of the 1500-cm^{-1} component by changing the laser power. The peak position of the 1500-cm^{-1} component is the same in all the spectra. We found that the intensity of the 1500-cm^{-1} component has a nonlinear power dependence. In Fig. 3(a), the peak intensities of the 1500-cm^{-1} scattering component in an undoped Ge sample are plotted against the exciting laser power in a log-log scale. The straight line in the figure represents a square-law dependence and is well fitted to the data points. This nonlinear power dependence suggests that the origin of the scattering should be related to some photoexcited product, such as photoexcited electrons or holes, because the increase of the laser power causes the carrier density to increase at the laser spot. At this stage, we can neglect the effects of collective excitations such as plasmons because we observed no change in the peak position, whereas the plasma frequency depends on the square root of the carrier density.

Similar experiments were made in p-type ($N_h = 10^{17}$ cm^{-3}) and n-type ($N_e = 10^{17}$ cm^{-3}) Ge crystals. The spectra of the 1500-cm^{-1} components in these samples under the 4 kW/cm^2 excitation were almost the same as that of the undoped sample shown in Fig. 1. The power dependence of the 1500-cm^{-1} component in the doped samples is shown in Fig. 3(b). In the n-type sample (open circles), the intensity also obeys the square law as shown in the figure. On the other hand, in the p-type sample (closed circles), it was found that the intensity has a square-law power dependence at high excitation densities, whereas it exhibits a linear power dependence below the critical point (~ 0.5 kW/cm^2). This result suggests that the origin of the 1500-cm^{-1} component should be related to holes in Ge.

We measured temperature dependence of the scattering intensity of the 1500-cm^{-1} component from RT to LNT. In these experiments, the excitation density was set to 8.2 kW/cm^2. Figure 4 shows the typical spectra at several temperatures. At 311 K, one can see a strong 1500-cm^{-1} component. As decreasing temperature, the intensity of the 1500-cm^{-1} component first increases slightly, reaching a maximum at ~200 K. Below 200 K, it decreases rapidly. Along with the de-

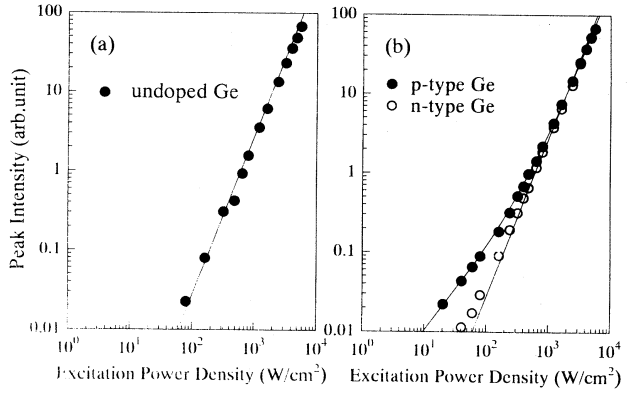

FIG. 3. (a) Laser power dependence of the Raman intensity of the 1500-cm^{-1} component in undoped Ge (circles). The straight line represents the square-law dependence on the laser power. (b) Laser power dependence of the Raman intensity of the 1500-cm^{-1} component in p-type Ge (closed circles) and n-type Ge (open circles). In the n-type sample, the power dependence is almost the same as in the undoped Ge. In the p-type sample, the Raman intensity changes linearly in the low power region. These measurements are successfully explained by Eq. (2), which was used in drawing the theoretical curves depicted by solid curves. Details are described in the text.

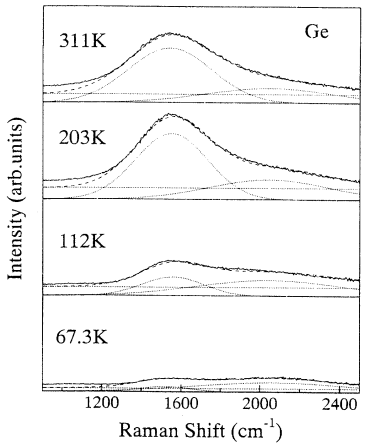

FIG. 4. Temperature dependence of the Raman spectrum around 1500 cm^{-1}. Excitation was made by 1.58-eV laser light with a power density of 8.2 kW/cm^2. The sample temperature was determined by the intensities of the LO-phonon lines. All the spectra can be successfully decomposed into two Gaussians and a constant base. The fitting results are depicted by the broken curves (total) and dotted curves (each component). The fitting parameters are summarized in Table II.

TABLE II. Spectral fitting parameters.

	1500-cm^{-1} component			2000-cm^{-1} component		
	Peak	Width	Peak intensity	Peak	Width	Peak intensity
311 K	1542	299	2.83	2043	467	0.77
203 K	1551	258	3.41	2043	433	1.04
112 K	1558	224	0.97	2043	527	0.82
67 K	1503	196	0.31	2043	517	0.55

crease, the shoulder in the high energy side around 2000 cm^{-1} becomes clear. At 67.3 K, the shoulder band dominates over the 1500-cm^{-1} component. As a first approximation, these spectra can be decomposed into two Gaussian bands (1500-cm^{-1} band and 2000-cm^{-1} band) and the base luminescence assumed as a constant. As shown by dotted curves in Fig. 4, they are well described by two Gaussian bands at all temperatures. Fitting results for the spectra shown in Fig. 4 are listed in Table II. One can see that the integrated intensity (intensity $\times$ width) of the side component around 2000-cm^{-1} is almost invariant with the temperature. Temperature dependence of the integrated intensity of the 1500-cm^{-1} component is depicted in Fig. 5. At 67.3 K, the intensity becomes 1/ 30 of the intensity at 200 K. Unlike the 1500-cm^{-1} component, the intensity of the 2000-cm^{-1} component hardly changes at all in this temperature range. This result suggests that the two bands have different scattering mechanisms.

IV. DISCUSSION

A. Origin of the 1500-cm^{-1} scattering component

The above results suggest that holes play an important role in the 1500-cm^{-1} scattering component. In this section, we try to consider the power dependence of the integrated intensity by a phenomenological model. Generally, the total hole density ρ_h in our sample can be represented by the sum of hole densities due to p-type doping (ρ_0) and to photoexcitation [αI_{laser}; I_{laser} represents the laser power density (W/cm^2)]. Assuming that the origin of the 1500-cm^{-1} component is holes, the intensity of the scattering should be proportional to the density of holes and the intensity of the laser. We can therefore express the intensity of Raman scattering as a function of the I_{laser} as follows:

$$I_{\text{Raman}} \propto I_{\text{laser}}\rho_h = I_{\text{laser}}(\rho_0 + \alpha I_{\text{laser}}) . \quad (2)$$

In the next section we deduce more quantitatively [Eq. (13)] that the Raman intensity should be proportional to the hole density ρ_h. In the special case for the undoped sample and the n-type sample, we can neglect the contribution of ρ_0, leading to a quadratic dependence on the laser power. This reproduces closely the experimental data of the undoped and n-type samples as shown by the straight lines in Figs. 3(a) and 3(b). If ρ_0 is nonzero (p-type sample), the intensity changes linearly as the power approaches zero and quadratically at the high power. The critical point of the laser power is given by $\rho_0 = \alpha I_{\text{laser}}$. This behavior seems to reproduce accurately the power dependence of the p-type sample (ρ_0=10^{17} cm^{-3}).

To check the above assumption more quantitatively, we estimate the hole density created by photoexcitation as follows. The density of holes under cw laser irradiation depends on several factors such as the laser power, spot size, diffusion constant, and the decay time of holes. We consider a simple model in which carriers are injected into a small point in the sample and diffuse isotropically with a diffusion constant of D while decaying with a lifetime of τ. The diffusion constant can be calculated from the mobility μ (Ref. 12) by using the Einstein relation $D = \mu k_B T$, which gives $D = 46$ cm^2 sec^{-1} at 300 K. The diffusion length is estimated as $\sqrt{D\tau} = 210$ μm, where $\tau = 10$ μs is the typical carrier lifetime at 300 K. This diffusion length is much larger than the laser spot size, which supports the small point injection model described above. The diffusion equation of photoexcited holes can be written as

$$\frac{\partial \rho(r)}{\partial t} = D\frac{1}{r^2}\frac{\partial}{\partial r}\left(r^2\frac{\partial}{\partial r}\right)\rho(r) - \frac{\rho(r)}{\tau} + \frac{n}{\pi^{1.5}R_0^3}\exp\left[-\left(\frac{r}{R_0}\right)^2\right] , \quad (3)$$

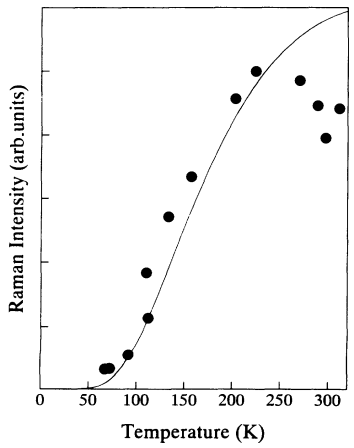

FIG. 5. Temperature dependence of the integrated intensity of the 1500-cm^{-1} component (closed circles). The fitting curve based on Eq. (13) is shown by the solid curve.

where $\rho(r)$ is the density of holes. The injection of carriers, the third term in Eq. (3), is assumed to have a Gaussian distribution (the width is R_0) in the radial direction with a total hole-injection rate of n per second. In our case, we should solve the steady-state equation, where $\partial\rho(r)/\partial t = 0$. By solving this equation with boundary conditions; $\rho(r \to \infty) = 0$ and $\rho(r \to 0) = finite$, one can obtain

$$\rho(r) = \frac{n}{8\pi D r}\exp\left(\frac{R_0^2}{4D\tau}\right)\left\{\exp\left(\frac{r}{\sqrt{D\tau}}\right)\left[Erf\left(\frac{r}{R_0}+\frac{R_0}{\sqrt{4D\tau}}\right)-1\right]+\exp\left(-\frac{r}{\sqrt{D\tau}}\right)\times\left[Erf\left(\frac{r}{R_0}-\frac{R_0}{\sqrt{4D\tau}}\right)+1\right]\right\}, \quad (4)$$

and when $R_0 \ll \sqrt{4D\tau}$,

$$\rho(0) = \frac{n}{2D\pi^{1.5}R_0}, \quad (5)$$

where $\rho(0)$ is the density of holes at the center of the laser spot. From the estimated diffusion length, the hole density within the laser spot is practically constant and can be estimated by Eq. (5). Assuming each photon creates one electron-hole pair, 1 W/cm^2 of 1.58-eV laser light makes 1.4×10^{14} holes per unit volume (cm^3) in our experimental conditions including reflection correction. The power dependence of the p-type sample can be reproduced by Eq. (2) with $\rho_0 = 6.4 \times 10^{16}$ cm^{-3} and $\alpha = 1.4 \times 10^{14}$ W^{-1}cm^{-1} as shown in Fig. 3(b). The critical point of the power dependence is given as 0.46 kW/cm^2. The value of ρ_0 obtained above is close to 10^{17} cm^{-3} of dopant in the p-type sample. At this point, we conclude that holes in Ge give rise to the 1500-cm^{-1} component.

B. Resonant inter-valence-band Raman scattering

In this section, we consider the mechanism of the light scattering of holes. The 1500-cm^{-1} Raman shift we obtained is too large to be attributed to the intraband nature such as CDF or SDF which should be observed below $\Delta q \cdot v_F$ (Δq=difference of the wave number between incident and scattered lights, v_F=Fermi velocity). In our case, $\Delta q \cdot v_F$ is less than ~100 cm^{-1}.[11] Considering this point, it is suggested that the origin of the 1500-cm^{-1} component should have the interband nature. To explain the Raman scattering of holes, we propose a model based on the resonant inter-valence-band Raman scattering (resonant IVRS) of holes from the HH band to the LH band. This is a process whereby an electron is photoexcited from the LH band to the intermediate state in the conduction band, and then makes a k-conserving transition to an empty valence state (hole) in the HH band, leaving behind an excited hole in the LH band.

In order to check this model, we first calculated the energy spectrum of holes in Ge near the Γ point by the $\vec{k}\cdot\vec{p}$ perturbation theory including spin and spin-orbit coupling[13,14] and evaluated the predicted Raman shift. As for the energy structure of holes in Ge, Lawaetz solved the second order $\vec{k}\cdot\vec{p}$ perturbation matrix for two special directions in k space; $\langle 100\rangle$ and $\langle 111\rangle$.[14] After Lawaetz, the energy spectrum of the HH band $E_h(\vec{k})$ and the energy spectrum of the LH band $E_l(\vec{k})$ for the $\langle 100\rangle$ direction can be expressed as

$$E_h(\vec{k}) = -(A-B)k^2, \quad (6)$$

$$E_l(\vec{k}) = -\frac{1}{2}\left[(2A+B)k^2+\Delta\right]+\left\{\frac{1}{4}\left[(2A+B)k^2+\Delta\right]^2-\Delta(A+B)k^2-(A+2B)(A-B)k^4\right\}^{\frac{1}{2}}. \quad (7)$$

For the $\langle 111\rangle$ direction, B is replaced by $D/\sqrt{3}$, where $D = (3B^2+C^2)^{\frac{1}{2}}$ and Δ represents the splitting energy at the Γ point between the LH band and the SO band, which is given by $\Delta = 0.295$ eV. The energy spectrum of the conduction band is given by

$$E_c(\vec{k}) = Ek^2 + E_{\rm gap}, \quad (8)$$

where $E_{\rm gap}$ is the direct gap energy at the Γ point. Parameters A, B, C, and E are referred to in the literature[14] and are listed in Table III in units of $\hbar^2/2m$ with $E_{\rm gap}$ in units of eV, where m is the free electron mass. Figure 6 shows the calculated band structure of Ge represented along the $\langle 100\rangle$ and $\langle 111\rangle$ direction. One of the resonant IVRS processes for $\hbar\omega_{\rm incident} = 1.58$ eV is also depicted by upward and downward arrows: an electron (closed circle) is excited from the LH band to the conduction band (E band) and deexcited to the HH band (abbreviated to LH $\to E \to$ HH). As a result, a hole (open circle) is excited from the HH band to the LH band. In this process, we ignore change of the wave vector by light scattering. Another resonant IVRS process such as SO $\to E \to$ HH may be also allowed, but it gives a Stokes shift far in excess of 2000 cm^{-1}, which means that the SO $\to E \to$ HH process is not relevant to this study.

In this model, the Raman spectrum is given by

$$I(\Delta\omega) \propto \sum_{i,f} P(E_i)\delta\left(\frac{E_i(\vec{k})-E_f(\vec{k})}{\hbar}-\Delta\omega\right)\left|\vec{e}_2(\overleftrightarrow{R})\vec{e}_1\right|^2, \quad (9)$$

$$(\overleftrightarrow{R})_{\mu\nu} = \frac{1}{m}\sum_n \frac{\langle f|\hat{p}_\mu|n\rangle\langle n|\hat{p}_\nu|i\rangle}{\hbar\omega_{\rm incident}-[E_n(\vec{k})-E_i(\vec{k})]+i\Gamma}, \quad (10)$$

where $\Delta\omega$ is the Raman shift, $|i\rangle$, $|n\rangle$, and $|f\rangle$ are wave

TABLE III. Band parameters.

A	B	$\lvert C\rvert$	E	$E_{\rm gap}$ (eV)
13.27	8.63	12.4	23.8	0.805

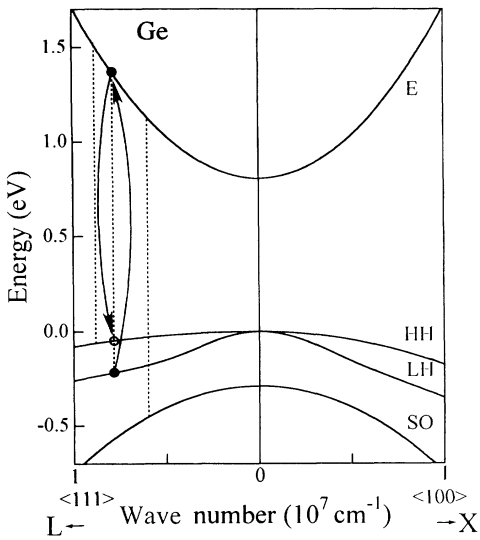

FIG. 6. Band structure in the ⟨111⟩ and ⟨100⟩ directions of Ge calculated by the $\vec{k}\cdot\vec{p}$ method after Lawaetz. The edges of the abscissa correspond to ~1/10 of the Brillouin zone. E, HH, LH, and SO stand for conduction, heavy hole, light hole, and splitoff hole bands. Dotted lines represent the photoexcitation paths under 1.58-eV photoexcitation: HH→ E at $k_A = 8.9\times10^6$ cm^{-1}, LH→ E at $k_A = 7.9\times10^6$ cm^{-1}, and SO→ E at $k_A = 6.0\times10^6$ cm^{-1}. Arrows describe the resonant IVRS process: an electron (closed circle) is excited from the LH band to the E band and deexcited to the HH band. As a result, a hole (open circle) is excited from the HH band to the LH band.

functions of the multiparticle system, and the energies of these states are represented by $E_i(\vec{k})$, $E_n(\vec{k})$, and $E_f(\vec{k})$. In our model, the intermediate state includes an excited electron in the conduction band and an excited hole in the LH band in addition to the thermally populated holes.

When we take into account only the resonant term in Eq. (10) and assume the k-conserving transition of the electron from the LH band to the conduction band and finally to the HH band, the Raman spectrum can be rewritten as

$$I(\Delta\omega)\propto\sum_{\vec{k}_A}\left|M_{\vec{k}_A}\right|^2 f_h(\hat{E}_h(\vec{k}_A))[1-f_l(\hat{E}_l(\vec{k}_A))] \times\delta\left(\frac{\hat{E}_l(\vec{k}_A)-\hat{E}_h(\vec{k}_A)}{\hbar}-\Delta\omega\right), \quad (11)$$

where $\vec{k}_A$ is the solution of the equation $\hbar\omega_{\text{incident}} - [E_c(\vec{k}) - E_l(\vec{k})] = 0$ and $\left|M_{\vec{k}_A}\right|^2$ contains the matrix elements. Here, we define the hole energies; $\hat{E}_h(\vec{k}) = -E_h(\vec{k})$ and $\hat{E}_l(\vec{k}) = -E_l(\vec{k})$. $f_h(\hat{E}_h)(f_l(\hat{E}_l))$ is the distribution function of holes in the HH band (LH band). The term $f_h(\hat{E}_h)[1-f_l(\hat{E}_l)]$ indicates that in the resonant IVRS process the initial state has holes in the HH band and no holes in the LH band with the same $\vec{k}$. The peak position of the Raman shift $\Delta\omega_0$ can be estimated by

$$\Delta\omega_0=\sum_{\vec{k}_A}P_{\vec{k}_A}\frac{\hat{E}_l(\vec{k}_A)-\hat{E}_h(\vec{k}_A)}{\hbar}, \quad (12)$$

where $P_{\vec{k}_A}$ is the normalized weight reflecting $f_h(1-f_l)\left|M_{\vec{k}_A}\right|^2$. In our case, where the Fermi energy (< 8 meV) is much smaller than the temperature, it is natural to assume that the holes obey a Boltzmann distribution. The term $1-f_l(\hat{E}_l)$ can be set to 1 for $\hat{E}_l = 1760$ cm^{-1} (2533 K) in this approximation. Using the effective mass approximation to calculate the chemical potential, the peak intensity I_0 is roughly estimated as

$$\begin{aligned} I_0 &\propto \sum_{\vec{k}_A}\left|M_{\vec{k}_A}\right|^2 f_h(\hat{E}_h(\vec{k}_A)) \\ &= \sum_{\vec{k}_A}\left|M_{\vec{k}_A}\right|^2 \exp\left(-\frac{\hat{E}_h(\vec{k}_A)-\mu}{k_BT}\right) \\ &\propto \sum_{\vec{k}_A}\rho_h\left|M_{\vec{k}_A}\right|^2 (k_BT)^{-1.5}\exp\left(-\frac{\hat{E}_h(\vec{k}_A)}{k_BT}\right), \end{aligned} \quad (13)$$

where ρ_h represents the total density of holes. Strictly speaking, we must execute the summation over all possible $\vec{k}_A$'s in Eqs. (12) and (13). However, within the framework of the $\vec{k}\cdot\vec{p}$ approximation, the splitting energy between HH and LH bands has a maximum in the $\vec{k}\parallel\langle111\rangle$ direction and a minimum in the $\vec{k}\parallel\langle100\rangle$ direction, whereas the energy difference between the E and LH bands is smallest in the $\vec{k}\parallel\langle111\rangle$ direction and largest in the $\vec{k}\parallel\langle100\rangle$ direction. This means that the Raman shift should be largest for holes with $\vec{k}\parallel\langle111\rangle$ and smallest for holes having $\vec{k}\parallel\langle100\rangle$. Therefore we only estimated the Raman shift in the cases of $\vec{k}\parallel\langle111\rangle$ and $\vec{k}\parallel\langle100\rangle$ by using analytic solutions of the second order $\vec{k}\cdot\vec{p}$ matrix including spin-orbit coupling. The calculated Raman shifts for laser photon energies corresponding to those in Fig. 2 are listed in Table I (third and fourth columns).

In order to estimate which direction is effective, we calculated the $\exp[-\hat{E}_h(\vec{k}_A)/k_BT]$ term in Eq. (13) at T =311 K,

$$\exp\left(-\frac{\hat{E}_h(\vec{k}_A\parallel\langle100\rangle)}{k_BT}\right)\Big/\exp\left(-\frac{\hat{E}_h(\vec{k}_A\parallel\langle111\rangle)}{k_BT}\right) = \exp\left(-\frac{1173}{311}\right)\Big/\exp\left(-\frac{561}{311}\right)=0.14\,.$$

This result means that the hole occupation number for $\vec{k}_A\parallel\langle111\rangle$—and therefore the Raman intensity due to holes in the ⟨111⟩ direction—is about one order of magnitude larger than that for $\vec{k}_A\parallel\langle100\rangle$. Taking this into account, we will only consider the holes in the ⟨111⟩ direction in the following discussion. As shown in Table I, the

model qualitatively explains the peak shifts with variation in excitation frequency, although the absolute values are a little smaller than the experimental results. Since the value of $\vec{k}_A$ is almost one-tenth of the zone width, deviations from the experimental results may be due to insufficient accuracy of the band calculations based on the $\vec{k} \cdot \vec{p}$ method. In this model, the broad scattering bandwidth originates from two sources: k-direction dependence of $\Delta\omega$, and the resonance width Γ given in Eq. (10) which reflects the relaxation process of excited holes.

This model can also be applied to the temperature dependence of the scattering intensity. We assumed ρ_h in Eq. (13) to be temperature invariant and fitted the data to Eq. (13). The solid curve in Fig. 5 shows a typical result calculated by using $T^{-1.5}\exp(-T_0/T)$, where $T_0 = \hat{E}_h(\vec{k}_A \parallel \langle 111\rangle)/k_B = 561$ K. The calculated curve closely reproduces the rapid decrease around 200 K in the experimental results. This result strongly supports our k-conserved resonant IVRS model. Deviation at high temperatures will come from the diffusion of carriers which reduces the hole density $\rho_h = \rho(0)$ as expected from Eq. (5).

Another way to explain the scattering mechanism is known as the non-k-conserved IVRS model, which was originally applied to p-GaAs by Olego *et al.*[10] We will briefly discuss on this model below. After Olego *et al.*, a non-k-conserving transition from the intermediate state to the final state is assumed. In this model, all the holes in the HH band contribute to the scattering. The Raman shift $\Delta\omega$ is roughly estimated as

$$\Delta\omega = \sum_{\vec{k}_A} P_{\vec{k}_A} \frac{\hat{E}_l(\vec{k}_A) - \hat{E}_F}{\hbar} , \tag{14}$$

where $\hat{E}_F$ is the Fermi energy of the holes. Calculation have also been done based on this model, and the results are listed in Table I (fifth and sixth column). The Fermi energy was calculated from the total hole density $\rho_h = 5 \times 10^{17}$ as $\hat{E}_F = 7.8$ meV under the effective mass approximation. This hole density corresponds to the highest density in our experimental condition, by which one can calculate the lower limit of the Raman shift. The non-k-conserving model gives slightly larger values than the experimental results. As for the peak shifts with the change of the exciting laser frequency, the non-k-conserving model is better than the k-conserving model, although the k-conserving model gives a more reasonable absolute value of the Raman shift. However, the non-k-conserving model has a serious problem that the model cannot explain the temperature dependence of the integrated intensity of the Raman spectrum: the integrated intensity of the IVRS in the non-k-conserving model has no temperature dependence because all the holes in the HH band contribute to the scattering.

In addition, our nominally undoped sample has an impurity of less than 10^{15} cm^{-3} which is much less than the hole density 10^{19} cm^{-3} in p-GaAs where the non-k-conserving model is assumed. Therefore, in our case with a nominally undoped sample, the dopant-induced non-k-conserving process should be suppressed. Furthermore, the observed Raman intensity of the 1500-cm^{-1} component in our doped samples is comparable to that in the undoped sample at high excitation (larger than 0.5 kW/cm^2), although the impurity density is higher by two orders of magnitude at least. These results strongly suggest that the non-k-conserving mechanism due to impurities does not play an important role in our case. From the two points mentioned above–temperature dependence and doping-level dependence–we conclude that the scattering mechanism of the 1500-cm^{-1} component should be the k-conserving resonant inter-valence-band scattering of holes.

We have no definite ideas on the origin of the side component that appears around 2000 cm^{-1} at low temperatures in Fig. 4. The 2000-cm^{-1} component is considered to behave differently from the 1500-cm^{-1} component. The experimental features, peak position (high energy side of the 1500-cm^{-1} component) and lack of temperature dependence, might suggest a non-k-conserving process. But it still remains to be determined why the 2000-cm^{-1} component appears not only in doped samples but also in the undoped sample.

V. CONCLUSION

We have observed broad Raman scattering around 1500 cm^{-1} in Ge. From the laser power dependence measured in undoped, n-type, and p-type samples, the origin of the Raman scattering is assigned as the holes in the valence band. We made band calculations based on the $\vec{k} \cdot \vec{p}$ method and estimated the peak position of the Raman scattering while assuming the k-conserving intervalence band scattering (IVRS) of holes. The temperature dependence of the integrated intensity of the scattering was also successfully explained by the k-conserving IVRS model. Such a k-conserving process has not been observed in ordinary heavily-p-doped systems, probably because of the efficient impurity-induced non-k-conserving process. We would like to stress that photo-doping techniques combined with the highly sensitive detection system used in this study allowed the study of carriers without influence of impurities.

As a possible application of carrier dynamics studies, time-resolved measurements of the k-conserving intervalence-band Raman scattering will be an alternative method to investigate the ultrafast relaxation of holes.

* Permanent address: Science University of Tokyo, Tokyo 162, Japan.
[1] M. Chandrasekhar, M. Cardona, and E. O. Kane, Phys. Rev. B **16**, 3579 (1977).
[2] I. P. Ipatova, A. V. Subashiev, and V. A. Voitenko, Solid State Commun. **37**, 893 (1981).
[3] D. A. Abramsohn, K. T. Tsen, and R. Bray, Phys. Rev. B **26**, 6571 (1982).
[4] G. Contreras, A. K. Sood, and M. Cardona, Phys. Rev. B **32**, 924 (1985).
[5] G. Contreras, A. K. Sood, and M. Cardona, Phys. Rev. B **32**, 930 (1985).
[6] N. Mestres and M. Cardona, Phys. Rev. Lett. **55**, 1132 (1985).
[7] K. Tanaka, H. Ohtake, and T. Suemoto, Phys. Rev. Lett. **71**, 1935 (1993).
[8] M. A. Kanehisa, R. F. Wallis, and M. Balkanski, Phys. Rev. B **25**, 7619 (1982).
[9] J. Wagner and M. Cardona, Phys. Rev. B **32**, 8071 (1985).
[10] D. Olego, M. Cardona, and U. Rössler, Phys. Rev. B **22**, 1905 (1980).
[11] M. V. Klein, in *Light Scattering in Solids I*, edited by M. Cardona (Springer-Verlag, Berlin, 1983), pp. 147–204.
[12] F. J. Morin, Phys. Rev. **93**, 62 (1954).
[13] G. Dresselhaus, A. F. Kip, and C. Kittel, Phys. Rev. **98**, 368 (1955).
[14] P. Lawaetz, Phys. Rev. **174**, 867 (1968).